Mixed and nonconforming finite element methods on a system of polygons ⋆

M. Vohralík [a] J. Maryška [a] O. Severýn [a]

[a] *Department of Modelling of Processes, Faculty of Mechatronics and Interdisciplinary Engineering Studies, Technical University of Liberec, Hálkova 6, 461 17 Liberec 1, Czech Republic*

Abstract

We investigate the lowest-order Raviart–Thomas mixed finite element method for second-order elliptic problems posed over a system of intersecting two-dimensional polygons placed in three-dimensional Euclidean space. Such problems arise for example in the context of groundwater flow through granitoid massifs, where the polygons represent the rock fractures. The domain is characteristic by the presence of intersection lines shared by three or more polygons. We first construct continuous and discrete function spaces ensuring the continuity of scalar functions and an appropriate continuity of the normal trace of vector functions across such intersection lines. We then propose a variant of the lowest-order Raviart–Thomas mixed finite element method for the given problem with the domain discretized into a triangular mesh and prove its well-posedness. We finally investigate the relation of the hybridization of the considered mixed finite element method to the piecewise linear nonconforming finite element method. We extend the results known in this direction onto networks of polygons, general diffusion tensors, and general boundary conditions. The obtained relation enables in particular an efficient implementation of the mixed finite element method. We finally verify the theoretical results on a model problem with a known analytical solution and show the application of the proposed method to the simulation of a real problem.

Key words: second-order elliptic problem, system of polygons, Raviart–Thomas mixed finite element method, nonconforming finite element method, fracture flow

⋆ This work was supported by the Grant Agency of the Czech Republic, grant No. 205/00/0480, and by the Ministry of Education of the Czech Republic, project code MSM 242200001.

Email addresses: martin.vohralik@tul.cz (M. Vohralík), jiri.maryska@tul.cz (J. Maryška), otto.severyn@tul.cz (O. Severýn).

1 Introduction

The motivation of this paper is the need to simulate water flow through underground rock massifs. Such massifs are proposed as e.g. nuclear waste repositories and they are always disrupted by a system of geological faults, *fractures*. One of the possible modeling approaches is to approximate the fractures by a network of planar polygonal disks whose frequency, size, assigned aperture, and orientation are statistically derived from field measurements, and to consider two-dimensional Darcy flow through such a network, see e.g. [1], [5], or [24]. This problem is mathematically a second-order elliptic problem posed over a system of intersecting two-dimensional polygons placed in three-dimensional Euclidean space. An example of such system is given in Figure 1. The system in this figure is already discretized into a triangular mesh. We can easily notice an essential property of a domain created by a system of polygons that is impossible in classical planar domains: there exist interelement edges in the triangulation which belong to three or more triangular elements.

We propose and investigate in this paper a variant of the lowest-order Raviart–Thomas mixed finite element method [19] (cf. also [7] or [20]) for systems of polygons. It turns out that the essential step is the definition of appropriate continuous and discrete function spaces: we have to ensure the continuity of the scalar primary unknown (pressure) across the intersection lines between polygons and an appropriate continuity of the normal trace of the flux of the primary unknown (the hydraulic conductivity tensor times the negative of the gradient of the pressure, i.e. the Darcy velocity) across these intersection lines. The well-posedness of the weak mixed formulation is then implied by the well-posedness of the weak primal formulation, which is easy to show. To demonstrate the existence and uniqueness of the mixed approximation, we define a global interpolation operator on the discrete velocity space and prove the commuting diagram property, which implies the discrete inf–sup condition. An extension to higher-order mixed finite element methods would be possible along the same lines.

We next investigate the relation of the hybridization of the lowest-order Raviart–Thomas mixed finite element method to the piecewise linear nonconforming finite element method. It is known that the matrices of these two methods coincide for an elliptic problem with an elementwise constant diffusion tensor and a homogeneous Dirichlet boundary condition, see [3] or a detailed study given in [9]. We extend these results onto systems of polygons, nonconstant diffusion tensors, and inhomogeneous mixed Dirichlet/Neumann boundary conditions. The implementation of the considered mixed finite element method via the nonconforming method is on the one hand very efficient and on the other hand, since a polygonal domain is a trivial instance of a system of polygons, is naturally valid also for standard planar domains. Such implementation in particular avoids the inverting of local matrices (cf. [7, Section V.1.2]), usually used when the relation with the nonconforming method is not known. Recall that inverting of local matrices is a potential source of significant numerical errors, cf. [12].

The outline of this paper is as follows. In Section 2 we formulate the second-order elliptic problem on a system of polygons and in Section 3 we define continuous and discrete function spaces on such system. We state the weak primal formulation and the nonconforming finite element approximation in Section 4. Section 5 is devoted to the lowest-order Raviart–Thomas mixed finite element method: we state and show the existence and uniqueness of the weak mixed solution and of the mixed approximation, introduce the hybridization of the mixed approximation, and give error estimates. Next, in Section 6 we investigate the relation between mixed and nonconforming methods. Finally, the first part of Section 7 presents the results of a numerical experiment on a model problem with a known analytical solution. The application of our method to realistic problems has been described in [17]; we give in the second part of Section 7 an example of a real problem simulation and briefly compare our approach with other methods. This paper is a detailed description of the results previously announced in [16] and [23].

2 Second-order elliptic problem on a system of polygons

We define the system of polygons $\mathcal{S}$ and the second-order elliptic problem on this system in this section. We set

$$\mathcal{S} := \left\{ \bigcup_{\ell \in L} \overline{\alpha_\ell} \setminus \partial\mathcal{S} \right\}, \tag{2.1}$$

where α_ℓ is an open two-dimensional polygon placed in three-dimensional space and L is the index set of polygons. We suppose that the closures $\overline{\alpha_\ell}$ of polygons are all connected into the system; the connection is only possible through an edge, not through a point. For the purpose of the mathematical description, we require that $\alpha_i \cap \alpha_j = \emptyset$ if $i \neq j$ and that $\overline{\alpha_i} \cap \overline{\alpha_j}$, $i \neq j$, is either an edge or a point or an empty set. In order to fulfill this property it is enough to divide each polygon from a general system of polygons as that of Figure 1 into subpolygons along each intersection line that it contains. Finally, $\partial\mathcal{S}$ is the set of those boundary points of α_ℓ, $\ell \in L$, which do not create the connection with other polygons. We suppose that there is a two-dimensional orthogonal coordinate system given in each polygon.

The problem of groundwater flow through fracture networks, see [1], reads as follows. We seek p (a scalar function in each $\overline{\alpha_\ell}$) and $\mathbf{u}$ (a two-dimensional vector in each $\overline{\alpha_\ell}$), the solutions of

$$\mathbf{u} = -\mathbf{K}(\nabla p + \nabla z) \quad \text{in } \alpha_\ell\,,\ \ell \in L\,, \tag{2.2a}$$

$$\nabla \cdot \mathbf{u} = q \quad \text{in } \alpha_\ell\,,\ \ell \in L\,, \tag{2.2b}$$

$$p = p_D \quad \text{on } \Gamma_D\,, \quad \mathbf{u}\cdot\mathbf{n} = u_N \quad \text{on } \Gamma_N\,. \tag{2.2c}$$

Here all the variables are expressed in the local two-dimensional coordinates of the

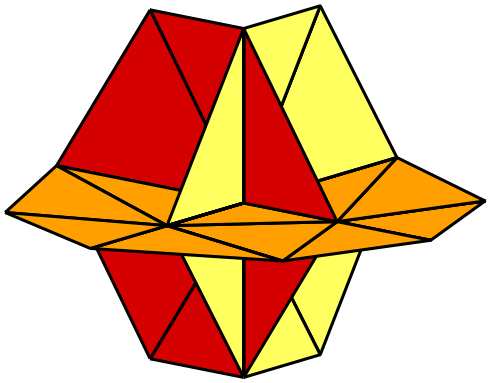

Fig. 1. Example of a simple system of polygons (discretized into a triangular mesh)

appropriate α_ℓ and ∇ and $\nabla\cdot$ are the gradient and divergence operators, respectively, with respect to these local coordinates. The variable p denotes the pressure head, $p = \hat{p}/\varrho g$, where $\hat{p}$ is the fluid pressure, g is the gravitational acceleration constant, and ϱ is the fluid density, $\mathbf{u}$ is the Darcy flow velocity, q represents stationary sources or sinks, z is the elevation, i.e. the upward vertical three-dimensional coordinate, and $\mathbf{K}$ is the tensor of hydraulic conductivity. The equation (2.2a) is then the Darcy law, (2.2b) is the mass balance equation, and (2.2c) prescribes Dirichlet and Neumann boundary conditions. Let f be an edge such that there exist polygons α_i and α_j, $i \neq j$, such that $f = \overline{\alpha_i} \cap \overline{\alpha_j}$. We denote the set of such edges by $\mathcal{E}^{\mathrm{int}}$ and the set of all $i \in L$ such that $f \subset \partial\alpha_i$ by I_f. The system (2.2a)–(2.2c) is completed by requiring

$$p|_{\overline{\alpha_i}} = p|_{\overline{\alpha_j}} \quad \text{on } f \qquad \forall f \in \mathcal{E}^{\mathrm{int}}\,,\ \forall i,j \in I_f\,, \tag{2.3a}$$

$$\sum_{i\in I_f} \mathbf{u}|_{\overline{\alpha_i}} \cdot \mathbf{n}_{f,\alpha_i} = 0 \quad \text{on } f \qquad \forall f \in \mathcal{E}^{\mathrm{int}}\,, \tag{2.3b}$$

where $\mathbf{n}_{f,\alpha_i}$ is the unit outward normal vector of the edge f with respect to the polygon α_i. The equations (2.3a)–(2.3b) express the continuity of p across the interpolygon boundaries and the mass balance of $\mathbf{u}$ across these boundaries (what is the outflow from one polygon has to be the inflow into the neighboring ones).

We finally suppose that $\Gamma_D \cap \Gamma_N = \emptyset$, $\overline{\Gamma_D} \cup \overline{\Gamma_N} = \partial\mathcal{S}$, that the measure of Γ_D is nonzero, and that $\mathbf{K}$ is a symmetric and uniformly positive definite tensor in each α_ℓ, i.e.

$$\mathbf{K}(\mathbf{x})\boldsymbol{\eta}\cdot\boldsymbol{\eta} \geq c_{\mathbf{K}}\boldsymbol{\eta}\cdot\boldsymbol{\eta}\,, \quad c_{\mathbf{K}} > 0\,, \tag{2.4}$$

for any $\boldsymbol{\eta} \in \mathbb{R}^2$ and almost all $\mathbf{x} \in \alpha_\ell$, for all $\ell \in L$.

3 Function spaces for nonconforming and mixed finite elements

We give in this section the definitions of function spaces used in the sequel. We will use the spaces $H^1(\alpha_\ell)$ and $\mathbf{H}(\mathrm{div}, \alpha_\ell)$ on separate polygons with certain matching

conditions at the interpolygon boundaries in order to define the spaces $H^1(\mathcal{S})$ and $\mathbf{H}(\mathrm{div},\mathcal{S})$ on the whole system $\mathcal{S}$. We introduce also the discrete counterparts of these spaces.

3.1 Continuous function spaces

We use the product of the spaces L^p, $1 \le p \le \infty$, on separate polygons in order to define the spaces $L^p(\mathcal{S})$ and $\mathbf{L}^p(S)$ on the system $\mathcal{S}$,

$$L^p(\mathcal{S}) := \prod_{\ell \in L} L^p(\alpha_\ell)\,, \quad \mathbf{L}^p(\mathcal{S}) := L^p(\mathcal{S}) \times L^p(\mathcal{S})\,. \tag{3.1}$$

For each polygon α_ℓ, we denote by $H^1(\alpha_\ell)$ the Sobolev space of scalar functions with square-integrable weak derivatives, $H^1(\alpha_\ell) = \{\varphi \in L^2(\alpha_\ell)\,;\, \nabla\varphi \in \mathbf{L}^2(\alpha_\ell)\}$. We define $H^1(\mathcal{S})$ as the space of functions whose restrictions to each α_ℓ are from $H^1(\alpha_\ell)$ and that coincide at the interpolygon boundaries in the sense of traces,

$$\begin{aligned} H^1(\mathcal{S}) := \Big\{ & v \in L^2(\mathcal{S})\,;\, v|_{\alpha_\ell} \in H^1(\alpha_\ell) \quad \forall \ell \in L\ , \\ & (v|_{\alpha_i})|_f = (v|_{\alpha_j})|_f \quad \forall f \in \mathcal{E}^{\mathrm{int}}\,,\, \forall i,j \in I_f \Big\}\ . \end{aligned} \tag{3.2}$$

We then have the space $H^1_D(\mathcal{S})$ of the functions from $H^1(\mathcal{S})$ vanishing on Γ_D and the spaces $H^{\frac{1}{2}}(\partial\mathcal{S})$, $H^{-\frac{1}{2}}(\partial\mathcal{S})$, $H^{\frac{1}{2}}(\Gamma_D)$, and $H^{-\frac{1}{2}}(\Gamma_N)$ as in the standard planar case.

For each polygon α_ℓ, we denote by $\mathbf{H}(\mathrm{div},\alpha_\ell)$ the space of vector functions with square-integrable weak divergences, $\mathbf{H}(\mathrm{div},\alpha_\ell) = \{\mathbf{v} \in \mathbf{L}^2(\alpha_\ell)\,;\, \nabla\cdot\mathbf{v} \in L^2(\alpha_\ell)\}$. We define $\mathbf{H}(\mathrm{div},\mathcal{S})$ as the space of functions whose restrictions to each α_ℓ are from $\mathbf{H}(\mathrm{div},\alpha_\ell)$ and whose sum of normal traces over all polygons sharing a given edge $f \in \mathcal{E}^{\mathrm{int}}$ is zero in the appropriate sense,

$$\begin{aligned} \mathbf{H}(\mathrm{div},\mathcal{S}) := \Big\{ & \mathbf{v} \in \mathbf{L}^2(\mathcal{S})\,;\, \mathbf{v}|_{\alpha_\ell} \in \mathbf{H}(\mathrm{div},\alpha_\ell) \quad \forall \ell \in L\,, \\ & \sum_{i \in I_f} \langle \mathbf{v}|_{\alpha_i} \cdot \mathbf{n}_{\partial\alpha_i}, \varphi_i\rangle_{\partial\alpha_i} = 0 \quad \forall \varphi_i \in H^1_{\partial\alpha_i \setminus f}(\alpha_i)\,, \\ & \varphi_i|_f = \varphi_j|_f \quad \forall i,j \in I_f\,,\, \forall f \in \mathcal{E}^{\mathrm{int}} \Big\}\,. \end{aligned} \tag{3.3}$$

Finally, we denote

$$\mathbf{H}_{0,N}(\mathrm{div},\mathcal{S}) := \Big\{ \mathbf{v} \in \mathbf{H}(\mathrm{div},\mathcal{S})\,;\, \langle \mathbf{v}\cdot\mathbf{n}, \varphi\rangle_{\partial\mathcal{S}} = 0 \quad \forall \varphi \in H^1_D(\mathcal{S}) \Big\}$$

as the space of functions from $\mathbf{H}(\mathrm{div},\mathcal{S})$ such that their normal trace on Γ_N is equal to zero in the appropriate sense.

We use $(\cdot,\cdot)_{0,\alpha_\ell}$ to denote the L^2 scalar product, $\|\cdot\|_{0,\alpha_\ell}$ to denote the associated L^2 norm, $\|\cdot\|_{1,\alpha_\ell}$ to denote the $H^1(\alpha_\ell)$ norm, and $\|\cdot\|_{\mathbf{H}(\mathrm{div},\alpha_\ell)}$ to denote the $\mathbf{H}(\mathrm{div},\alpha_\ell)$ norm given by $\|\mathbf{v}\|^2_{\mathbf{H}(\mathrm{div},\alpha_\ell)} = \|\mathbf{v}\|^2_{0,\alpha_\ell} + \|\nabla\cdot\mathbf{v}\|^2_{0,\alpha_\ell}$. The bracket $\langle \mathbf{v}\cdot\mathbf{n}, \varphi\rangle_{\partial\mathcal{S}}$ denotes the duality pairing between $H^{-\frac{1}{2}}(\partial\mathcal{S})$ and $H^{\frac{1}{2}}(\partial\mathcal{S})$ and may be written formally as $\int_{\partial\mathcal{S}} \mathbf{v}\cdot\mathbf{n}\,\varphi\,\mathrm{d}\gamma(\mathbf{x})$. The norms on the spaces defined by (3.1), (3.2), and (3.3) are given by

$$\|\cdot\|^2_{\cdot,\mathcal{S}} := \sum_{\ell\in L} \|\cdot\|^2_{\cdot,\alpha_\ell}\,. \tag{3.4}$$

Remark 3.1 (Continuity across the interpolygon boundaries) *The definitions (3.2) and (3.3) express weakly the conditions (2.3a) and (2.3b). Let $\Omega\subset\mathbb{R}^2$ be a polygonal domain and let $\mathcal{S}$ be its polygonal partition. Then the definitions (3.2) and (3.3) coincide with the standard characterizations of $H^1(\Omega)$ and $\mathbf{H}(\mathrm{div},\Omega)$ (cf. [7, Propositions III.1.1 and III.1.2] or [20, Theorem 1.3]).*

Throughout this paper, we shall suppose that $\mathbf{K}_{ij}\in L^\infty(\mathcal{S})$, $q\in L_2(\mathcal{S})$, $p_D\in H^{\frac{1}{2}}(\Gamma_D)$, and $u_N\in H^{-\frac{1}{2}}(\Gamma_N)$.

3.2 Discrete function spaces

Let us suppose a triangulation $\mathcal{T}_h$ of the system $\mathcal{S}$ such that the boundary edges lie entirely either in Γ_D or in Γ_N. We set

$$M^0_{-1}(\mathcal{T}_h) := \left\{ \phi\in L^2(\mathcal{S})\,;\, \phi|_e \text{ is constant } \forall e\in\mathcal{T}_h \right\}.$$

We denote the set of all edges of $\mathcal{T}_h$ by $\mathcal{E}_h$, the set of all edges of $\mathcal{T}_h$ except those from Γ_D by $\mathcal{E}_{h,D}$, and the set of all interior edges of $\mathcal{T}_h$ by $\mathcal{E}_h^{\mathrm{int}}$. We set

$$\begin{aligned} M^0_{-1}(\mathcal{E}_{h,D}) := \{\, &\mu:\mathcal{E}_h\to\mathbb{R}\,;\, \mu|_f \text{ is constant } \forall f\in\mathcal{E}_h\,,\\ &\mu|_f = 0 \quad \forall f\subset\Gamma_D\,\}\,. \end{aligned}$$

For the nonconforming approximation, we set

$$X^1_0(\mathcal{E}_h) := \left\{\varphi\in L^2(\mathcal{S});\ \varphi|_e \text{ is linear } \forall e\in\mathcal{T}_h\,,\ \varphi \text{ is continuous in } Q_f, f\in\mathcal{E}_h^{\mathrm{int}}\right\},$$

where Q_f is the midpoint of the edge f. The basis of $X^1_0(\mathcal{E}_h)$ is spanned by shape functions φ_f, $f\in\mathcal{E}_h$, such that $\varphi_f(Q_g)=\delta_{fg}$, $g\in\mathcal{E}_h$, δ being the Kronecker delta. A simple computation gives

$$\nabla\varphi_f|_e = \frac{|f|}{|e|}\mathbf{n}_f \qquad e\in\mathcal{T}_h\,,\ f\subset\partial e\,, \tag{3.5}$$

where $|e|$ is the area of the element e, $|f|$ is the length of the edge f, and $\mathbf{n}_f$ is the unit normal vector of the edge f, outward to e. We finally set

$$X_0^1(\mathcal{E}_{h,D}) := \left\{ \varphi \in X_0^1(\mathcal{E}_h);\, \varphi(Q_f) = 0 \quad \forall f \subset \Gamma_D \right\} .$$

For a given triangular element $e \in \mathcal{T}_h$, we define $\mathbf{RT}^0(e)$ as the space of linear vector functions with the basis $\mathbf{v}_i^e$, $i = 1, 2, 3$,

$$\mathbf{v}_i^e(\mathbf{x}) := \frac{1}{2|e|} \begin{pmatrix} x - x_i \\ y - y_i \end{pmatrix} \text{ if } \mathbf{x} = (x, y)^t \in e\,, \quad \mathbf{v}_i^e(\mathbf{x}) := \begin{pmatrix} 0 \\ 0 \end{pmatrix} \text{ if } \mathbf{x} \notin e\,, \tag{3.6}$$

where $(x_i, y_i)^t$ are the coordinates of the i-th vertex of e. Note that $\mathbf{v}_i^e \cdot \mathbf{n}_f$ is constant over each edge $f \subset \partial e$. The Raviart–Thomas space $\mathbf{RT}_{-1}^0(\mathcal{T}_h)$ of elementwise linear vector functions without any continuity requirement is defined by

$$\mathbf{RT}_{-1}^0(\mathcal{T}_h) := \left\{ \mathbf{v} \in \mathbf{L}^2(\mathcal{S})\,;\, \mathbf{v}|_e \in \mathbf{RT}^0(e) \quad \forall e \in \mathcal{T}_h \right\} . \tag{3.7}$$

We set the space $\mathbf{RT}_0^0(\mathcal{T}_h)$ of functions ensuring the normal trace continuity as

$$\begin{aligned} \mathbf{RT}_0^0(\mathcal{T}_h) &:= \left\{ \mathbf{v} \in \mathbf{RT}_{-1}^0(\mathcal{T}_h)\,;\, \sum_{e \in \mathcal{T}_h\,; f \subset \partial e} \mathbf{v}|_e \cdot \mathbf{n}_{f,e} = 0 \text{ on } f \quad \forall f \in \mathcal{E}_h^{\text{int}} \right\} \\ &= \mathbf{RT}_{-1}^0(\mathcal{T}_h) \cap \mathbf{H}(\mathrm{div}, \mathcal{S})\,. \end{aligned} \tag{3.8}$$

To characterize the discrete functions with zero normal trace on Γ_N, we finally set

$$\mathbf{RT}_{0,N}^0(\mathcal{T}_h) := \left\{ \mathbf{v} \in \mathbf{RT}_0^0(\mathcal{T}_h)\,;\, \mathbf{v} \cdot \mathbf{n} = 0 \text{ on } \Gamma_N \right\} = \mathbf{RT}_{-1}^0(\mathcal{T}_h) \cap \mathbf{H}_{0,N}(\mathrm{div}, \mathcal{S})\,.$$

4 Nonconforming finite element method

We introduce in this section a weak primal solution of the problem (2.2a)–(2.3b). We next define its piecewise linear nonconforming finite element approximation.

4.1 Weak primal solution

Let $\tilde{p} \in H^1(\mathcal{S})$ be such that $\tilde{p} = p_D$ on Γ_D in the sense of traces. We then define:

Definition 4.1 (Weak primal solution) *As the weak primal solution of the problem (2.2a)–(2.3b), we understand a function $p = p_0 + \tilde{p}$, $p_0 \in H_D^1(\mathcal{S})$, satisfying*

$$(\mathbf{K}\nabla p_0, \nabla\varphi)_{0,\mathcal{S}} = (q,\varphi)_{0,\mathcal{S}} - \langle u_N, \varphi\rangle_{\partial\mathcal{S}} - (\mathbf{K}\nabla z, \nabla\varphi)_{0,\mathcal{S}} \\ -(\mathbf{K}\nabla\tilde{p}, \nabla\varphi)_{0,\mathcal{S}} \qquad \forall\varphi \in H^1_D(\mathcal{S})\,. \tag{4.1}$$

Existence and uniqueness of the weak primal solution follow from (2.4) and from the definition of the norms on $\mathcal{S}$ given by (3.4) using the Lax–Milgram lemma. The Friedrichs inequality generalized to systems of polygons,

$$\|\varphi\|_{0,\mathcal{S}} \le C_{\mathrm{F}}\|\nabla\varphi\|_{0,\mathcal{S}} \qquad \forall\varphi \in H^1_D(\mathcal{S})\,, \tag{4.2}$$

is necessary in this respect. We thus briefly sketch its proof. As the system $\mathcal{S}$ consists of a finite number of polygons, there exists a shape-regular triangulation $\mathcal{T}_h$ of $\mathcal{S}$ satisfying the inverse assumption (the size of all elements in $\mathcal{T}_h$ is comparable). Let the space $W_D(\mathcal{T}_h)$ be formed by functions locally in $H^1(e)$ on each triangle $e \in \mathcal{T}_h$ such that the mean values of their traces on interior edges coincide and such that the mean values of the traces on edges belonging to Γ_D are equal to zero. Clearly, $H^1_D(\mathcal{S}) \subset W_D(\mathcal{T}_h)$. Since the discrete Friedrichs inequality on the space $W_D(\mathcal{T}_h)$ is a straightforward extension of [22, Lemma V.4.5], also the Friedrichs inequality (4.2) holds true.

4.2 Nonconforming finite element approximation

We now turn to the piecewise linear nonconforming finite element approximation. It reads as follows:

Definition 4.2 (Nonconforming finite element approximation) *As the piecewise linear nonconforming finite element approximation of the problem (4.1), we understand a function $p_h = p_{0,h} + \tilde{p}$, $p_{0,h} \in X^1_0(\mathcal{E}_{h,D})$, satisfying*

$$\sum_{e\in\mathcal{T}_h} (\mathbf{K}\nabla p_{0,h}, \nabla\varphi_h)_{0,e} = \sum_{e\in\mathcal{T}_h} \{(q,\varphi_h)_{0,e} - \langle u_N, \varphi_h\rangle_{\partial e\cap\partial\mathcal{S}} - (\mathbf{K}\nabla z, \nabla\varphi_h)_{0,e} \\ - (\mathbf{K}\nabla\tilde{p}, \nabla\varphi_h)_{0,e}\} \qquad \forall\varphi_h \in X^1_0(\mathcal{E}_{h,D})\,. \tag{4.3}$$

Existence and uniqueness of the nonconforming approximation follow by the same arguments as above. Alternatively, the fact that the stiffness matrix arising from the nonconforming discretization is invertible can easily be shown as follows: let $\mathbb{S}$ be the nonconforming finite element stiffness matrix given by $\mathbb{S}_{f,g} = \sum_{e\in\mathcal{T}_h}(\mathbf{K}\nabla\varphi_g, \nabla\varphi_f)_{0,e}$, $f, g \in \mathcal{E}_{h,D}$. Let the vector X given by X_f, $f \in \mathcal{E}_{h,D}$, be nonzero and let $p_{0,h} = \sum_{f\in\mathcal{E}_{h,D}} X_f\varphi_f$. Then

$$X^t\mathbb{S}X = \sum_{f\in\mathcal{E}_{h,D}}\sum_{g\in\mathcal{E}_{h,D}} X_f X_g \mathbb{S}_{f,g} = \sum_{e\in\mathcal{T}_h} (\mathbf{K}\nabla p_{0,h}, \nabla p_{0,h})_{0,e} \ge c_{\mathbf{K}} \sum_{e\in\mathcal{T}_h} \|\nabla p_{0,h}\|^2_{0,e} > 0\,,$$

using (2.4) and since $\sum_{e\in\mathcal{T}_h}\|\nabla p_{0,h}\|_{0,e}^2$ is only zero when $p_{0,h}=0$ (i.e. when $X=0$) owing to the fact that $p_{0,h}(Q_f)=0$ for all $f\subset\Gamma_D$ (that is, $\{\sum_{e\in\mathcal{T}_h}\|\nabla(\cdot)\|_{0,e}^2\}^{\frac12}$ is a norm on $X_0^1(\mathcal{E}_{h,D})$).

5 Raviart–Thomas mixed finite element method

We first define in this section a weak mixed solution of the problem (2.2a)–(2.3b) and show its existence and uniqueness. We then study its lowest-order Raviart–Thomas mixed finite element approximation. We finally introduce its hybridization and give error estimates.

5.1 Weak mixed solution

Let $\tilde{\mathbf{u}}\in\mathbf{H}(\mathrm{div},\mathcal{S})$ be such that $\tilde{\mathbf{u}}\cdot\mathbf{n}=u_N$ on Γ_N in the appropriate sense. We then define:

Definition 5.1 (Weak mixed solution) *As the weak mixed solution of the problem (2.2a)–(2.3b), we understand functions* $\mathbf{u}=\mathbf{u}_0+\tilde{\mathbf{u}}$, $\mathbf{u}_0\in\mathbf{H}_{0,N}(\mathrm{div},\mathcal{S})$, *and* $p\in L^2(\mathcal{S})$ *such that*

$$\begin{aligned}(\mathbf{K}^{-1}\mathbf{u}_0,\mathbf{v})_{0,\mathcal{S}}-(\nabla\cdot\mathbf{v},p)_{0,\mathcal{S}}&=-\langle\mathbf{v}\cdot\mathbf{n},p_D\rangle_{\partial\mathcal{S}}+(\nabla\cdot\mathbf{v},z)_{0,\mathcal{S}}\\ -\langle\mathbf{v}\cdot\mathbf{n},z\rangle_{\partial\mathcal{S}}-(\mathbf{K}^{-1}\tilde{\mathbf{u}},\mathbf{v})_{0,\mathcal{S}}&\qquad\forall\,\mathbf{v}\in\mathbf{H}_{0,N}(\mathrm{div},\mathcal{S})\,,\end{aligned}\tag{5.1a}$$

$$-(\nabla\cdot\mathbf{u}_0,\phi)_{0,\mathcal{S}}=-(q,\phi)_{0,\mathcal{S}}+(\nabla\cdot\tilde{\mathbf{u}},\phi)_{0,\mathcal{S}}\qquad\forall\phi\in L^2(\mathcal{S})\,.\tag{5.1b}$$

Theorem 5.2 (Existence and uniqueness of the weak mixed solution) *The problem (5.1a)–(5.1b) has a unique solution.*

PROOF. The coercivity of the bilinear form $(\mathbf{K}^{-1}\mathbf{u},\mathbf{v})_{0,\mathcal{S}}$, $\mathbf{u},\mathbf{v}\in\mathbf{H}_{0,N}(\mathrm{div},\mathcal{S})$, on the space $\mathbf{W}=\{\mathbf{v}\in\mathbf{H}_{0,N}(\mathrm{div},\mathcal{S})\,;\,(\nabla\cdot\mathbf{v},\phi)_{0,\mathcal{S}}=0\quad\forall\phi\in L^2(\mathcal{S})\}$ is the consequence of the uniform positive definiteness of the tensor $\mathbf{K}$ on each α_ℓ given by (2.4). Next, we prove below that the divergence operator from $\mathbf{H}_{0,N}(\mathrm{div},\mathcal{S})$ to $L^2(\mathcal{S})$ is surjective (and hence the inf–sup condition). Thus the existence and uniqueness of the weak mixed solution are guaranteed by [7, Theorem II.1.1] or [20, Theorem 10.1].

To prove the desired surjectivity, we have to show that for all $q\in L^2(\mathcal{S})$ there exists $\mathbf{v}\in\mathbf{H}_{0,N}(\mathrm{div},\mathcal{S})$ such that $(\nabla\cdot\mathbf{v},\phi)_{0,\mathcal{S}}=(q,\phi)_{0,\mathcal{S}}$ for all $\phi\in L^2(\mathcal{S})$. Let thus $q\in L^2(\mathcal{S})$ be given and let us consider the problem of finding $p\in H_D^1(\mathcal{S})$ such that

$$(\nabla p,\nabla\varphi)_{0,\mathcal{S}}=(q,\varphi)_{0,\mathcal{S}}\qquad\forall\varphi\in H_D^1(\mathcal{S})\,.\tag{5.2}$$

The existence and uniqueness of such p follow by the well-posedness of the weak primal formulation given in Section 4.1. We affirm that the searched $\mathbf{v}$ is given by $\mathbf{v} = -\nabla p$. To prove this, we have to show that $\nabla p \in \mathbf{H}_{0,N}(\mathrm{div}, \mathcal{S})$ and that $-\nabla \cdot \nabla p = q$ in the appropriate sense. The second assertion is a simple consequence of (5.2), considering $\varphi \in H^1_0(\alpha_\ell)$, $\ell \in L$, as test functions in (5.2). We now proceed to show the first assertion. Let us consider an edge $f \in \mathcal{E}^{\mathrm{int}}$. We take $\varphi \in H^1_D(\mathcal{S})$ such that φ only has as a support the polygons sharing the edge f and such that φ is zero on $\partial\alpha_i \setminus f$ for all $i \in I_f$ in the sense of traces. The second assertion gives $\nabla p|_{\alpha_\ell} \in \mathbf{H}(\mathrm{div}, \alpha_\ell)$, $\ell \in L$, and $-\sum_{i\in I_f}(\nabla \cdot \nabla p, \varphi)_{0,\alpha_i} = (q, \varphi)_{0,\mathcal{S}}$. Hence, using the Green theorem on each polygon in (5.2) with the considered φ as the test function,

$$
\begin{aligned}
0 = \sum_{i\in I_f} (\nabla p, \nabla\varphi)_{0,\alpha_i} - (q,\varphi)_{0,\mathcal{S}} = \sum_{i\in I_f} \langle \nabla p|_{\alpha_i} \cdot \mathbf{n}_{\partial\alpha_i}, \varphi\rangle_{\partial\alpha_i} \\
- \sum_{i\in I_f} (\nabla \cdot \nabla p, \varphi)_{0,\alpha_i} - (q,\varphi)_{0,\mathcal{S}} = \sum_{i\in I_f} \langle \nabla p|_{\alpha_i} \cdot \mathbf{n}_{\partial\alpha_i}, \varphi\rangle_{\partial\alpha_i} \,,
\end{aligned}
$$

which by the fact that $\varphi \in H^1(\mathcal{S})$ implies that $\nabla p \in \mathbf{H}(\mathrm{div}, \mathcal{S})$, cf. the definition (3.3). Finally, $\nabla p \in \mathbf{H}_{0,N}(\mathrm{div}, \mathcal{S})$ follows by the above technique applied to (5.2). □

5.2 Properties of the discrete velocity space

We begin with the space $\mathbf{RT}^0(e)$ for a given $e \in \mathcal{T}_h$. Its basis is given by (3.6). The dual basis to this basis is given by the functionals N^e_j, $j = 1, 2, 3$, where

$$
N^e_j(\mathbf{u}) = \int_{f^e_j} \mathbf{u} \cdot \mathbf{n}_{\partial e} \, \mathrm{d}\gamma(\mathbf{x}) \qquad \mathbf{u} \in \mathbf{RT}^0(e) \,.
$$

Each N^e_j expresses the flux of $\mathbf{u}$ through one edge f^e_j of e. The local interpolation operator is then given by

$$
\pi_e(\mathbf{u}) = \sum_{i=1}^{3} N^e_i(\mathbf{u}) \mathbf{v}^e_i \qquad \mathbf{u} \in (H^1(e))^2 \,. \tag{5.3}
$$

We now turn to the problem of finding the basis and the dual basis of $\mathbf{RT}^0_0(\mathcal{T}_h)$. Let us consider $\mathbf{u} \in \mathbf{RT}^0_0(\mathcal{T}_h)$. We set $\mathcal{N}_h = \{N_1, N_2, \ldots, N_{|I_{\mathcal{N}_h}|}\}$, where for each boundary edge f such that $f \subset \partial e$, we define one functional N_f by

$$
N_f(\mathbf{u}) := \int_f \mathbf{u}|_e \cdot \mathbf{n}_{\partial e} \, \mathrm{d}\gamma(\mathbf{x}) \,,
$$

and for each interior edge f shared by the elements $e_1, e_2, \ldots, e_{|I_f|}$, we define $|I_f| - 1$

functionals by

$$N_{f,j}(\mathbf{u}) := \frac{1}{|I_f|}\int_f \mathbf{u}|_{e_1}\cdot\mathbf{n}_{\partial e_1}\,\mathrm{d}\gamma(\mathbf{x}) - \frac{1}{|I_f|}\int_f \mathbf{u}|_{e_{j+1}}\cdot\mathbf{n}_{\partial e_{j+1}}\,\mathrm{d}\gamma(\mathbf{x})\,,\quad j=1,\ldots,|I_f|-1\,.$$

We use the same denotation I_f for the index set of polygons sharing a given edge $f\in\mathcal{E}^{\mathrm{int}}$ in the continuous case and for the index set of elements sharing a given edge $f\in\mathcal{E}_h^{\mathrm{int}}$ in the discrete case. We have the following lemma:

Lemma 5.3 (Basis of the dual space to $\mathbf{RT}_0^0(\mathcal{T}_h)$) *$\mathcal{N}_h$ is a basis of the dual space to $\mathbf{RT}_0^0(\mathcal{T}_h)$.*

PROOF. To prove the lemma it suffices to show that for all $\mathbf{u}\in\mathbf{RT}_0^0(\mathcal{T}_h)$, from $N_j(\mathbf{u})=0\ \forall\, j=1,\ldots,|I_{\mathcal{N}_h}|$, it follows that $\mathbf{u}=0$. Let us suppose that $N_j(\mathbf{u})=0\ \forall\, j=1,\ldots,|I_{\mathcal{N}_h}|$. From the definition of the functionals N_f on boundary edges, we have $\int_f \mathbf{u}|_e\cdot\mathbf{n}_{\partial e}\,\mathrm{d}\gamma(\mathbf{x})=0$ for all boundary edges f. Using the definition of the functionals $N_{f,j}$ on interior edges, we have $\int_f \mathbf{u}|_{e_1}\cdot\mathbf{n}_{\partial e_1}\,\mathrm{d}\gamma(\mathbf{x}) = \int_f \mathbf{u}|_{e_j}\cdot\mathbf{n}_{\partial e_j}\,\mathrm{d}\gamma(\mathbf{x})$ for all $j=2,\ldots,|I_f|$. Considering the equality $\sum_{i\in I_f}\int_f \mathbf{u}|_{e_i}\cdot\mathbf{n}_{\partial e_i}\,\mathrm{d}\gamma(\mathbf{x})=0$ characterizing the continuity of the normal trace of the functions from $\mathbf{RT}_0^0(\mathcal{T}_h)$, cf. the definition (3.8), we come to $\int_f \mathbf{u}|_e\cdot\mathbf{n}_{\partial e}\,\mathrm{d}\gamma(\mathbf{x})=0$ for all $f\in\mathcal{E}_h$ and all e, $f\subset\partial e$. Since $\mathbf{RT}_0^0(\mathcal{T}_h)\subset\mathbf{RT}_{-1}^0(\mathcal{T}_h)$, $\mathbf{u}=0$ follows. □

We set $\mathcal{V}_h=\{\mathbf{v}_1,\mathbf{v}_2,\ldots,\mathbf{v}_{|I_{\mathcal{N}_h}|}\}$, the basis of $\mathbf{RT}_0^0(\mathcal{T}_h)$, in the following way: we define one basis function $\mathbf{v}_f$ by $\mathbf{v}_f:=\mathbf{v}_f^e$ for each boundary edge f. Here $\mathbf{v}_f^e$ is the local basis function associated with the element e and its edge f. For each interior edge f shared by the elements $e_1,e_2,\ldots,e_{|I_f|}$, we define $|I_f|-1$ basis functions by

$$\mathbf{v}_{f,i} := \sum_{k=1,\,k\neq i+1}^{|I_f|}\mathbf{v}_f^{e_k} - (|I_f|-1)\mathbf{v}_f^{e_{i+1}}\,,\quad i=1,\ldots,|I_f|-1\,.$$

Note that by the definition (3.8) of $\mathbf{RT}_0^0(\mathcal{T}_h)$, there is one condition imposed on each interior edge, so that the number of basis functions of $\mathbf{RT}_{-1}^0(\mathcal{T}_h)$ is decreased by one on each interior edge to obtain the appropriate continuity of the normal trace. When $|I_f|=2$, we have the classical basis function. An example of one of the two basis functions for three elements with the same edge is given in Figure 2. We have the following lemma:

Lemma 5.4 (Duality) *$\mathcal{V}_h$ is the dual basis to $\mathcal{N}_h$.*

PROOF. We have to show that $N_j(\mathbf{v}_i)=\delta_{ij}$, $i,j=1,\ldots,|I_{\mathcal{N}_h}|$. We have from the definition of the basis functions of $\mathbf{RT}^0(e)$ that $N_f(\mathbf{v}_f)=1$ for all boundary edges f, and simply $N_f(\mathbf{v})=0$ for all $\mathbf{v}\in\mathcal{V}_h$, $\mathbf{v}\neq\mathbf{v}_f$. Concerning the interior edges, we easily come to $N_{f,j}(\mathbf{v}_g)=0$ for all $j=1,\ldots,|I_f|-1$, f an interior edge, g a boundary edge,

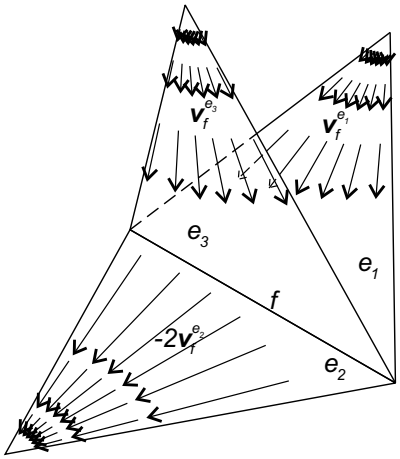

Fig. 2. Velocity basis function for three elements sharing the same edge

and to $N_{f,j}(\mathbf{v}_{g,i}) = 0$ for all $j = 1, \ldots, |I_f| - 1$, $i = 1, \ldots, |I_g| - 1$, f an interior edge, g another interior edge. We have

$$N_{f,j}(\mathbf{v}_{f,i}) = \frac{1}{|I_f|} \int_f \mathbf{v}_f^{e_1} \cdot \mathbf{n}_{\partial e_1} \, \mathrm{d}\gamma(\mathbf{x}) - \frac{1}{|I_f|} \int_f \mathbf{v}_f^{e_{j+1}} \cdot \mathbf{n}_{\partial e_{j+1}} \, \mathrm{d}\gamma(\mathbf{x}) = \frac{1}{|I_f|} - \frac{1}{|I_f|} = 0$$

for $i \neq j$ and

$$\begin{aligned} N_{f,i}(\mathbf{v}_{f,i}) &= \frac{1}{|I_f|} \int_f \mathbf{v}_f^{e_1} \cdot \mathbf{n}_{\partial e_1} \, \mathrm{d}\gamma(\mathbf{x}) - \frac{1}{|I_f|} \int_f -(|I_f| - 1) \mathbf{v}_f^{e_{i+1}} \cdot \mathbf{n}_{\partial e_{i+1}} \, \mathrm{d}\gamma(\mathbf{x}) \\ &= \frac{1}{|I_f|} + \frac{1}{|I_f|}(|I_f| - 1) = 1 \end{aligned}$$

for $i = 1, \ldots, |I_f| - 1$, f an interior edge. Thus the proof is completed. $\square$

We are now ready to define the global interpolation operator. We introduce first a space smoother than $\mathbf{H}(\mathrm{div}, \mathcal{S})$,

$$\begin{aligned} \mathbf{H}(\mathrm{grad}, \mathcal{S}) := \Big\{ & v \in \mathbf{L}^2(\mathcal{S}) \, ; \, \mathbf{v}|_{\alpha_\ell} \in (H^1(\alpha_\ell))^2 \quad \forall \ell \in L \, , \\ & \sum_{i \in I_f} \mathbf{v}|_{\alpha_i} \cdot \mathbf{n}_{f,\alpha_i} = 0 \ \text{ on } f \quad \forall f \in \mathcal{E}^{\mathrm{int}} \Big\} . \end{aligned} \tag{5.4}$$

We then define the global interpolation operator π_h by

$$\pi_h(\mathbf{u}) := \sum_{i=1}^{|I_{\mathcal{N}_h}|} N_i(\mathbf{u}) \mathbf{v}_i \qquad \mathbf{u} \in \mathbf{H}(\mathrm{grad}, \mathcal{S}) \, . \tag{5.5}$$

We have the following relation between π_e and π_h:

Lemma 5.5 (Equality between local and global interpolation operators) *The local and global interpolation operators defined by (5.3) and (5.5), respectively, equal on each element, i.e.*

$$\pi_h(\mathbf{u})|_e = \pi_e(\mathbf{u}|_e) \qquad \forall e \in \mathcal{T}_h,\, \forall\, \mathbf{u} \in \mathbf{H}(\mathrm{grad}, \mathcal{S})\,.$$

PROOF. As the basis functions $\mathbf{v}_i$, $i = 1, \ldots, |I_{\mathcal{N}_h}|$, of $\mathbf{RT}_0^0(\mathcal{T}_h)$ are combined from the local basis functions $\mathbf{v}_j^e$ on each element, we only have to verify that the coefficients of $\mathbf{v}_j^e$ are the same. For boundary edges, the coefficients for both local and global interpolation operators are equally given by $\int_f \mathbf{u}|_e \cdot \mathbf{n}_{\partial e}\, \mathrm{d}\gamma(\mathbf{x})$. For an interior edge f, we have for the global interpolation operator

$$\begin{aligned}
&\Big\{ \sum_{i=1}^{|I_f|-1} N_{f,i}(\mathbf{u}) \mathbf{v}_{f,i} \Big\}\Big|_{e_j} = \Big\{ \sum_{i=1}^{|I_f|-1} \Big(\frac{1}{|I_f|} \int_f \mathbf{u}|_{e_1} \cdot \mathbf{n}_{\partial e_1}\, \mathrm{d}\gamma(\mathbf{x}) \\
&- \frac{1}{|I_f|} \int_f \mathbf{u}|_{e_{i+1}} \cdot \mathbf{n}_{\partial e_{i+1}}\, \mathrm{d}\gamma(\mathbf{x}) \Big) \Big(\sum_{k=1,\, k\neq i+1}^{|I_f|} \mathbf{v}_f^{e_k} - (|I_f|-1)\mathbf{v}_f^{e_{i+1}} \Big) \Big\} \Big|_{e_j} \\
= &\sum_{i=1,\, i\neq j-1}^{|I_f|-1} \Big(\frac{1}{|I_f|} \int_f \mathbf{u}|_{e_1} \cdot \mathbf{n}_{\partial e_1}\, \mathrm{d}\gamma(\mathbf{x}) - \frac{1}{|I_f|} \int_f \mathbf{u}|_{e_{i+1}} \cdot \mathbf{n}_{\partial e_{i+1}}\, \mathrm{d}\gamma(\mathbf{x}) \Big) \mathbf{v}_f^{e_j} \\
&-(1-\delta_{j1}) \Big(\frac{1}{|I_f|} \int_f \mathbf{u}|_{e_1} \cdot \mathbf{n}_{\partial e_1}\, \mathrm{d}\gamma(\mathbf{x}) - \frac{1}{|I_f|} \int_f \mathbf{u}|_{e_j} \cdot \mathbf{n}_{\partial e_j}\, \mathrm{d}\gamma(\mathbf{x}) \Big) (|I_f|-1) \mathbf{v}_f^{e_j}
\end{aligned}$$

using the definition of $N_{f,i}$ and $\mathbf{v}_{f,i}$, $i = 1, \ldots, |I_f| - 1$, $j = 1, \ldots, |I_f|$. Considering now only the coefficients of $\mathbf{v}_f^{e_j}$, we come to

$$\begin{aligned}
&\sum_{i=1}^{|I_f|-1} \frac{1}{|I_f|} \int_f \mathbf{u}|_{e_1} \cdot \mathbf{n}_{\partial e_1}\, \mathrm{d}\gamma(\mathbf{x}) - \sum_{i=1}^{|I_f|-1} \frac{1}{|I_f|} \int_f \mathbf{u}|_{e_{i+1}} \cdot \mathbf{n}_{\partial e_{i+1}}\, \mathrm{d}\gamma(\mathbf{x}) \\
= &\Big((|I_f|-1)\frac{1}{|I_f|} + \frac{1}{|I_f|} \Big) \int_f \mathbf{u}|_{e_1} \cdot \mathbf{n}_{\partial e_1}\, \mathrm{d}\gamma(\mathbf{x}) = \int_f \mathbf{u}|_{e_1} \cdot \mathbf{n}_{\partial e_1}\, \mathrm{d}\gamma(\mathbf{x})
\end{aligned}$$

for $j = 1$, using the normal trace continuity of $\mathbf{u}$, which is expressed by $\sum_{i=1}^{|I_f|} \int_f \mathbf{u}|_{e_i} \cdot \mathbf{n}_{\partial e_i}\, \mathrm{d}\gamma(\mathbf{x}) = 0$. Similarly,

$$\begin{aligned}
&(|I_f|-2)\frac{1}{|I_f|} \int_f \mathbf{u}|_{e_1} \cdot \mathbf{n}_{\partial e_1}\, \mathrm{d}\gamma(\mathbf{x}) + \frac{1}{|I_f|} \int_f \mathbf{u}|_{e_1} \cdot \mathbf{n}_{\partial e_1}\, \mathrm{d}\gamma(\mathbf{x}) \\
&+\frac{1}{|I_f|} \int_f \mathbf{u}|_{e_j} \cdot \mathbf{n}_{\partial e_j}\, \mathrm{d}\gamma(\mathbf{x}) - (|I_f|-1)\frac{1}{|I_f|} \int_f \mathbf{u}|_{e_1} \cdot \mathbf{n}_{\partial e_1}\, \mathrm{d}\gamma(\mathbf{x}) \\
&+(|I_f|-1)\frac{1}{|I_f|} \int_f \mathbf{u}|_{e_j} \cdot \mathbf{n}_{\partial e_j}\, \mathrm{d}\gamma(\mathbf{x}) = \int_f \mathbf{u}|_{e_j} \cdot \mathbf{n}_{\partial e_j}\, \mathrm{d}\gamma(\mathbf{x})
\end{aligned}$$

for $j \geq 2$, and thus the proof is completed. $\square$

We conclude this section by the following theorem:

Theorem 5.6 (Commuting diagram property) *The commuting diagram property holds, i.e.*

$$\begin{array}{ccc} \mathbf{H}(\mathrm{grad},\mathcal{S}) & \xrightarrow{\mathrm{div}} & L^2(\mathcal{S}) \\ \Big\downarrow \pi_h & & \Big\downarrow P_h \\ \mathbf{RT}_0^0(\mathcal{T}_h) & \xrightarrow{\mathrm{div}} & M_{-1}^0(\mathcal{T}_h) \end{array} ,$$

where π_h is the global interpolation operator defined by (5.5) and P_h is the $L^2(\mathcal{S})$-orthogonal projection onto $M_{-1}^0(\mathcal{T}_h)$.

PROOF. The proof is immediate using the previous lemma and the validity of the commuting diagram property for the local interpolation operator, see e.g. [7, Proposition III.3.7] or [18, Section 3.4.2]. □

5.3 Mixed finite element approximation

We are ready to define the mixed approximation:

Definition 5.7 (Mixed finite element approximation) *As the lowest-order Raviart–Thomas mixed finite element approximation of the problem (5.1a)–(5.1b), we understand functions $\mathbf{u}_h = \mathbf{u}_{0,h} + \tilde{\mathbf{u}}$, $\mathbf{u}_{0,h} \in \mathbf{RT}_{0,N}^0(\mathcal{T}_h)$, and $p_h \in M_{-1}^0(\mathcal{T}_h)$ satisfying*

$$\begin{aligned} (\mathbf{K}^{-1}\mathbf{u}_{0,h}, \mathbf{v}_h)_{0,\mathcal{S}} - (\nabla\cdot\mathbf{v}_h, p_h)_{0,\mathcal{S}} &= -\langle \mathbf{v}_h\cdot\mathbf{n}, p_D\rangle_{\partial\mathcal{S}} + (\nabla\cdot\mathbf{v}_h, z)_{0,\mathcal{S}} \\ -\langle \mathbf{v}_h\cdot\mathbf{n}, z\rangle_{\partial\mathcal{S}} - (\mathbf{K}^{-1}\tilde{\mathbf{u}}, \mathbf{v}_h)_{0,\mathcal{S}} &\qquad \forall\, \mathbf{v}_h \in \mathbf{RT}_{0,N}^0(\mathcal{T}_h)\,, \end{aligned} \tag{5.6a}$$

$$-(\nabla\cdot\mathbf{u}_{0,h}, \phi_h)_{0,\mathcal{S}} = -(q,\phi_h)_{0,\mathcal{S}} + (\nabla\cdot\tilde{\mathbf{u}}, \phi_h)_{0,\mathcal{S}} \qquad \forall \phi_h \in M_{-1}^0(\mathcal{T}_h)\,. \tag{5.6b}$$

The commuting diagram property expressed by Theorem 5.6 implies the discrete inf–sup condition, which in turn ensures that the problem (5.6a)–(5.6b) has a unique solution.

5.4 Hybridization of the mixed approximation

We will now introduce the hybridization of the mixed approximation:

Definition 5.8 (Hybridization of the mixed approximation) *As the hybridization of the lowest-order Raviart–Thomas mixed finite element approximation of the*

problem (5.1a)–(5.1b), we understand functions $\mathbf{u}_h = \mathbf{u}_{0,h} + \tilde{\mathbf{u}}$, $\mathbf{u}_{0,h} \in \mathbf{RT}^0_{-1}(\mathcal{T}_h)$, $p_h \in M^0_{-1}(\mathcal{T}_h)$, *and* $\lambda_h \in M^0_{-1}(\mathcal{E}_{h,D})$ *satisfying*

$$\begin{aligned}
&\sum_{e\in\mathcal{T}_h} \Big\{(\mathbf{K}^{-1}\mathbf{u}_{0,h}, \mathbf{v}_h)_{0,e} - (\nabla\cdot\mathbf{v}_h, p_h)_{0,e} + \langle \mathbf{v}_h\cdot\mathbf{n}, \lambda_h\rangle_{\partial e}\Big\} \\
&= \sum_{e\in\mathcal{T}_h} \Big\{-\langle \mathbf{v}_h\cdot\mathbf{n}, p_D\rangle_{\partial e\cap\Gamma_D} + (\nabla\cdot\mathbf{v}_h, z)_{0,e} - \langle \mathbf{v}_h\cdot\mathbf{n}, z\rangle_{\partial e} - (\mathbf{K}^{-1}\tilde{\mathbf{u}}, \mathbf{v}_h)_{0,e}\Big\} \quad (5.7a) \\
&\qquad\qquad \forall\, \mathbf{v}_h \in \mathbf{RT}^0_{-1}(\mathcal{T}_h)\,,
\end{aligned}$$

$$\begin{aligned}
-\sum_{e\in\mathcal{T}_h} (\nabla\cdot\mathbf{u}_{0,h}, \phi_h)_{0,e} &= -\sum_{e\in\mathcal{T}_h} \{(q,\phi_h)_{0,e} - (\nabla\cdot\tilde{\mathbf{u}}, \phi_h)_{0,e}\} \\
&\forall \phi_h \in M^0_{-1}(\mathcal{T}_h)\,, \qquad (5.7b)
\end{aligned}$$

$$\sum_{e\in\mathcal{T}_h} \langle \mathbf{u}_{0,h}\cdot\mathbf{n}, \mu_h\rangle_{\partial e} = 0 \qquad \forall \mu_h \in M^0_{-1}(\mathcal{E}_{h,D})\,. \qquad (5.7c)$$

It is immediate that if $\mathbf{v}_h \in \mathbf{RT}^0_{-1}(\mathcal{T}_h)$, then $\mathbf{v}_h \in \mathbf{RT}^0_{0,N}(\mathcal{T}_h)$ if and only if

$$\sum_{e\in\mathcal{T}_h} \langle \mathbf{v}_h\cdot\mathbf{n}, \lambda_h\rangle_{\partial e} = 0 \qquad \forall \lambda_h \in M^0_{-1}(\mathcal{E}_{h,D})\,.$$

This ensures that the triple $\mathbf{u}_{0,h}$, p_h, λ_h exists and is unique and that $\mathbf{u}_{0,h}$ and p_h are at the same time the unique solutions of (5.6a)–(5.6b). We summarize the previous developments in the following theorem:

Theorem 5.9 (Existence and uniqueness of the mixed-hybrid approximation) *The problem (5.7a)–(5.7c) has a unique solution.*

5.5 Error estimates

We now give two error estimates, following from the classical interpolation theory. If the solution $(\mathbf{u}, p)$ of (5.1a)–(5.1b) is smooth enough and if $(\mathbf{u}_h, p_h, \lambda_h)$ is the solution of (5.7a)–(5.7c), we have

$$\|\mathbf{u} - \mathbf{u}_h\|_{\mathbf{H}(\mathrm{div},\mathcal{S})} + \|p - p_h\|_{0,\mathcal{S}} \le Ch(\|p\|_{1,\mathcal{S}} + \|\mathbf{u}\|_{1,\mathcal{S}} + \|q\|_{1,\mathcal{S}})\,,$$

where the constant C does not depend on h (see [7, Proposition IV.1.2]).

Using the piecewise linear but nonconforming approximation $\tilde{\lambda}_h \in X^1_0(\mathcal{E}_h)$ given by the values of the Lagrange multiplier λ_h at the midpoints of the edges, we have (see [7,

Theorem V.3.1])

$$\|p - \tilde{\lambda}_h\|_{0,\mathcal{S}} \le Ch^2(\|p\|_{1,\mathcal{S}} + \|\mathbf{u}\|_{1,\mathcal{S}} + \|q\|_{1,\mathcal{S}})\,.$$

6 Relation between mixed and nonconforming methods

We study in this section the relation between the hybridization of the lowest-order Raviart–Thomas mixed finite element method and the nonconforming method. We extend the results of [9] onto systems of polygons, general diffusion tensors, and general boundary conditions. This also enables us to efficiently implement the mixed finite element method in the considered case.

6.1 Algebraic condensation of the mixed-hybrid approximation

Let us denote, for all $e \in \mathcal{T}_h$,

$$\mathbf{u}_{0,h}|_e = \begin{pmatrix} a_e + c_e x \\ b_e + c_e y \end{pmatrix}\,, \quad p_h|_e = p_e$$

and similarly, for all $f \in \mathcal{E}_h$,

$$\lambda_h|_f = \lambda_f\,.$$

We now follow the ideas of [9]. Let $e \in \mathcal{T}_h$ be fixed. Consider in (5.7b) a test function ϕ_h equal to 1 on e and zero otherwise. This gives $c_e = q_e/2 - \tilde{\mathbf{u}}_e/2$ with

$$q_e := \frac{\int_e q\,\mathrm{d}\mathbf{x}}{|e|}\,, \quad \tilde{\mathbf{u}}_e := \frac{\int_e \nabla\cdot\tilde{\mathbf{u}}\,\mathrm{d}\mathbf{x}}{|e|}\,. \tag{6.1}$$

Next consider in (5.7a) two test functions, $\mathbf{v}_h = (1,0)^t$, $\mathbf{v}_h = (0,1)^t$ on e and zero otherwise, whose divergence is apparently zero. This gives

$$\int_e \mathbf{K}^{-1}\mathbf{u}_{0,h}\,\mathrm{d}\mathbf{x} + \int_{\partial e} \lambda_h\,\mathbf{n}\,\mathrm{d}\gamma(\mathbf{x}) = \mathbf{r}_e$$

with

$$\mathbf{r}_e := -\int_{\partial e\cap\Gamma_D} p_D\,\mathbf{n}\,\mathrm{d}\gamma(\mathbf{x}) - \int_{\partial e} z\,\mathbf{n}\,\mathrm{d}\gamma(\mathbf{x}) - \int_e \mathbf{K}^{-1}\tilde{\mathbf{u}}\,\mathrm{d}\mathbf{x}\,.$$

Let $\tilde{\lambda}_h \in X_0^1(\mathcal{E}_{h,D})$ be given by

$$\tilde{\lambda}_h := \sum_{f\in\mathcal{E}_h} \lambda_f\varphi_f\,.$$

Then using (3.5), we have

$$\int_{\partial e} \lambda_h \, \mathbf{n} \, \mathrm{d}\gamma(\mathbf{x}) = \sum_{f \subset \partial e} \lambda_f |f| \mathbf{n}_f = |e| \sum_{f \in \partial e} \lambda_f \nabla \varphi_f|_e = |e| \, \nabla \tilde{\lambda}_h|_e \, .$$

Next,

$$\int_e \mathbf{K}^{-1} \mathbf{u}_{0,h} \, \mathrm{d}\mathbf{x} = \int_e \mathbf{K}^{-1} \, \mathrm{d}\mathbf{x} \begin{pmatrix} a_e \\ b_e \end{pmatrix} + c_e \int_e \mathbf{K}^{-1} \begin{pmatrix} x \\ y \end{pmatrix} \, \mathrm{d}\mathbf{x} \, .$$

Let us denote

$$\mathbf{K}_e := \Big(\frac{1}{|e|} \int_e \mathbf{K}^{-1} \, \mathrm{d}\mathbf{x} \Big)^{-1} \qquad e \in \mathcal{T}_h \, . \tag{6.2}$$

Then the above equations give

$$\begin{pmatrix} a_e \\ b_e \end{pmatrix} + c_e \frac{\mathbf{K}_e}{|e|} \int_e \mathbf{K}^{-1} \begin{pmatrix} x \\ y \end{pmatrix} \, \mathrm{d}\mathbf{x} + \mathbf{K}_e \nabla \tilde{\lambda}_h|_e = \mathbf{K}_e \frac{\mathbf{r}_e}{|e|}$$

and consequently

$$\begin{aligned} \mathbf{u}_{0,h}|_e = -\mathbf{K}_e \nabla \tilde{\lambda}_h|_e + \Big[\frac{q_e}{2} - \frac{\tilde{\mathbf{u}}_e}{2} \Big] \Bigg[\begin{pmatrix} x \\ y \end{pmatrix} \\ - \frac{\mathbf{K}_e}{|e|} \int_e \mathbf{K}^{-1} \begin{pmatrix} x \\ y \end{pmatrix} \, \mathrm{d}\mathbf{x} \Bigg] + \mathbf{K}_e \frac{\mathbf{r}_e}{|e|} \, . \end{aligned} \tag{6.3}$$

We finally substitute (6.3) into (5.7c). This gives the following system of linear equations with the only unknowns the Lagrange multipliers λ_h:

$$\begin{aligned} \sum_{e \in \mathcal{T}_h} (\mathbf{K}_e \nabla \tilde{\lambda}_h, \nabla \tilde{\mu}_h)_{0,e} = \sum_{e \in \mathcal{T}_h} \Bigg\langle \Bigg\{ \Big[\frac{q_e}{2} - \frac{\tilde{\mathbf{u}}_e}{2} \Big] \Bigg[\begin{pmatrix} x \\ y \end{pmatrix} \\ - \frac{\mathbf{K}_e}{|e|} \int_e \mathbf{K}^{-1} \begin{pmatrix} x \\ y \end{pmatrix} \, \mathrm{d}\mathbf{x} \Bigg] + \mathbf{K}_e \frac{\mathbf{r}_e}{|e|} \Bigg\} \cdot \mathbf{n}, \mu_h \Bigg\rangle_{\partial e} \qquad \forall \mu_h \in M^0_{-1}(\mathcal{E}_{h,D}) \, , \end{aligned} \tag{6.4}$$

where $\tilde{\mu}_h \in X^1_0(\mathcal{E}_{h,D})$ is given by

$$\tilde{\mu}_h := \sum_{f \in \mathcal{E}_h} \mu_f \varphi_f \, .$$

The left-hand side of (6.4) follows by

$$\langle \mathbf{K}_e \nabla \tilde{\lambda}_h|_e \cdot \mathbf{n}, \mu_h \rangle_{\partial e} = \langle \mathbf{K}_e \nabla \tilde{\lambda}_h|_e \cdot \mathbf{n}, \tilde{\mu}_h \rangle_{\partial e} = (\mathbf{K}_e \nabla \tilde{\lambda}_h, \nabla \tilde{\mu}_h)_{0,e} \qquad \forall e \in \mathcal{T}_h \, .$$

Here, we have used the fact that $\mathbf{K}_e \nabla \tilde{\lambda}_h|_e \cdot \mathbf{n}\, \mu_h$ is constant over each edge and hence its integral over this edge equals to that of $\mathbf{K}_e \nabla \tilde{\lambda}_h|_e \cdot \mathbf{n}\, \tilde{\mu}_h$, which is a linear function with the same value at the edge midpoint by the definition of $\tilde{\mu}_h$, and finally the Green theorem in e (notice that $\mathbf{K}_e \nabla \tilde{\lambda}_h|_e$ is a constant vector in e and hence its divergence is zero).

The system given by (6.4), in the sequel called (algebraically) *condensed mixed-hybrid method*, enables a very efficient implementation of the scheme (5.7a)–(5.7c). In particular, its system matrix is symmetric and positive definite and the number of unknowns equals to the number of interior and Neumann boundary edges; remark that this number does not increase with the number of triangles sharing the given edge. Moreover, this matrix is assembled directly and one thus can avoid the inverting of local matrices, which is necessary in the traditional static condensation approach (cf. [7, Section V.1.2]). It is pointed out in [12] that the inverting of local matrices is a potential source of significant numerical errors. Finally, note that the velocity $\mathbf{u}_{0,h} \in \mathbf{RT}^0_{0,N}(\mathcal{T}_h)$ is easily obtained from the knowledge of $\tilde{\lambda}_h$ by (6.3). It is easily seen that the system (6.4) is very close to that given by the nonconforming finite element approximation (4.3). We give detailed comments on the relation between these two systems in the next section.

6.2 Comparison of condensed mixed-hybrid and nonconforming methods

We consider in this section the detailed relation between the condensed mixed-hybrid finite element method given by (6.4) and the nonconforming finite element method given by (4.3). We consider the matrices of the problems and the different parts of the right-hand sides separately.

System matrix

It is easily seen from (6.4), (4.3), and (6.2) that the system matrix of the condensed mixed-hybrid method is the system matrix of the nonconforming method with a piecewise constant diffusion tensor, given as the inverse of the elementwise average of the inverse of the original one. In particular, for elementwise constant diffusion tensors, these matrices coincide, as it was already shown in [9]. Simply, the mixed-hybrid method employs the harmonic average of the hydraulic conductivity tensor, whereas the nonconforming method uses instead the arithmetic average.

Sources term

Using the simple trick of replacing μ_h by $\tilde{\mu}_h$ and the Green theorem in each $e \in \mathcal{T}_h$ as at the end of Section 6.1, we have for the sources term of the condensed mixed-hybrid

method the expression

$$\sum_{e\in\mathcal{T}_h}(q_e,\tilde{\mu}_h)_{0,e}+\sum_{e\in\mathcal{T}_h}\frac{q_e}{2}\left(\begin{pmatrix}x_e\\y_e\end{pmatrix}-\frac{\mathbf{K}_e}{|e|}\int_e\mathbf{K}^{-1}\begin{pmatrix}x\\y\end{pmatrix}\,\mathrm{d}\mathbf{x},\nabla\tilde{\mu}_h\right)_{0,e},$$

where $(x_e,y_e)^t$ are the coordinates of the barycentre of the triangle e. In particular, if $\mathbf{K}$ is elementwise constant, the second term of the above expression vanishes. Hence the essential difference with the source term of the nonconforming method is the employment of the elementwise average of q given by (6.1) rather than taking q directly.

Dirichlet boundary condition term

Let the function p_D be smooth enough and let us consider the usual approximation $\tilde{p}\approx\sum_{f\subset\Gamma_D}p_D(Q_f)\varphi_f$. Then the Dirichlet boundary condition term in the nonconforming method becomes

$$-\sum_{e\in\mathcal{T}_h}(\mathbf{K}\nabla\tilde{p},\nabla\tilde{\mu}_h)_{0,e}\approx-\sum_{e\in\mathcal{T}_h}\left(\mathbf{K}\sum_{f\subset\partial e\cap\Gamma_D}p_D(Q_f)\frac{|f|}{|e|}\mathbf{n}_f,\nabla\tilde{\mu}_h\right)_{0,e},$$

where $\tilde{\mu}_h\in X_0^1(\mathcal{E}_{h,D})$ and where we have employed the relation (3.5). This is obviously equivalent, up to replacing $\mathbf{K}$ by $\mathbf{K}_e$, to the expression for this term from the condensed mixed-hybrid method

$$-\sum_{e\in\mathcal{T}_h}\left(\frac{\mathbf{K}_e}{|e|}\int_{\partial e\cap\Gamma_D}p_D\,\mathbf{n}\,\mathrm{d}\gamma(\mathbf{x}),\nabla\tilde{\mu}_h\right)_{0,e}\approx-\sum_{e\in\mathcal{T}_h}\left(\frac{\mathbf{K}_e}{|e|}\sum_{f\subset\partial e\cap\Gamma_D}p_D(Q_f)|f|\mathbf{n}_f,\nabla\tilde{\mu}_h\right)_{0,e}.$$

Neumann boundary condition term

Let us for simplicity consider just one edge f where the Neumann boundary condition is prescribed, i.e. $\Gamma_N=f$. Then the Neumann boundary condition term in the nonconforming method, with the usual approximation supposing that u_N is smooth enough and for the test function φ_f, is

$$-\int_f u_N\varphi_f\,\mathrm{d}\gamma(\mathbf{x})\approx-\int_f u_N(Q_f)\varphi_f\,\mathrm{d}\gamma(\mathbf{x})=-u_N(Q_f)|f|\,.$$

Recall that this term equals to zero for all other test functions φ_g, $g\in\mathcal{E}_{h,D}$, $g\neq f$.

Using the same techniques as in the above paragraphs, we can express the Neumann boundary condition term in the condensed mixed-hybrid method as

$$
- \sum_{e\in\mathcal{T}_h} (\tilde{\mathbf{u}}_e, \tilde{\mu}_h)_{0,e} - \sum_{e\in\mathcal{T}_h} \frac{\tilde{\mathbf{u}}_e}{2} \left(\begin{pmatrix} x_e \\ y_e \end{pmatrix} - \frac{\mathbf{K}_e}{|e|} \int_e \mathbf{K}^{-1} \begin{pmatrix} x \\ y \end{pmatrix} \,\mathrm{d}\mathbf{x}, \nabla\tilde{\mu}_h \right)_{0,e}
$$
$$
- \sum_{e\in\mathcal{T}_h} \left\langle \left\{ \frac{\mathbf{K}_e}{|e|} \int_e \mathbf{K}^{-1}\tilde{\mathbf{u}} \,\mathrm{d}\mathbf{x} \right\} \cdot \mathbf{n}, \mu_h \right\rangle_{\partial e} .
$$

Let $\mathbf{K}$ be elementwise constant; then the second term of the above expression vanishes and its third term simplifies. Let $e \in \mathcal{T}_h$ be such that $f \subset \partial e$ and let us finally consider the usual approximation $\tilde{\mathbf{u}} \approx u_N(Q_f)|f|\mathbf{v}_f^e$, where $\mathbf{v}_f^e \in \mathbf{RT}^0(e)$ is the local velocity basis function associated with the element e and its edge f. Then this term is a priori nonzero only for e and for the three test functions φ_g, $g \subset \partial e$, and has the form

$$
-\frac{u_N(Q_f)|f|}{|e|} \left(\int_e \nabla\cdot\mathbf{v}_f^e \,\mathrm{d}\mathbf{x}, \varphi_g \right)_{0,e} - \frac{u_N(Q_f)|f|}{|e|} \left\langle \left\{ \int_e \mathbf{v}_f^e \,\mathrm{d}\mathbf{x} \right\} \cdot \mathbf{n}, \varphi_g \right\rangle_{\partial e} .
$$

A simple computation gives

$$
\int_e \nabla\cdot\mathbf{v}_f^e \,\mathrm{d}\mathbf{x} = 1 \,, \quad \int_e \mathbf{v}_f^e \,\mathrm{d}\mathbf{x} = \frac{1}{2}\mathbf{w} \,,
$$

where $\mathbf{w} = (x_e, y_e)^t - (x_f, y_f)^t$ with $(x_f, y_f)^t$ being the coordinates of the vertex of e opposite to f. This finally gives for the Neumann boundary condition term in the condensed mixed-hybrid method, using simple geometrical properties of a triangle,

$$
-\frac{u_N(Q_f)|f|}{3} - \frac{u_N(Q_f)|f||g|}{2|e|}\mathbf{w}\cdot\mathbf{n}_g = -u_N(Q_f)|f|\delta_{f,g} \,,
$$

which coincides with the expression from the nonconforming method.

Gravity term

Using that the gradient of z is piecewise constant, a development similar to that for the Dirichlet boundary condition gives that the expressions for the gravity term from the nonconforming and condensed mixed-hybrid methods differ just by the employment of $\mathbf{K}$, $\mathbf{K}_e$, respectively.

7 Numerical experiments

We present in this section the results of a numerical experiment on a model problem with a known analytical solution. We then describe the application of the proposed method to the simulation of real fracture flow and compare it with other methods.

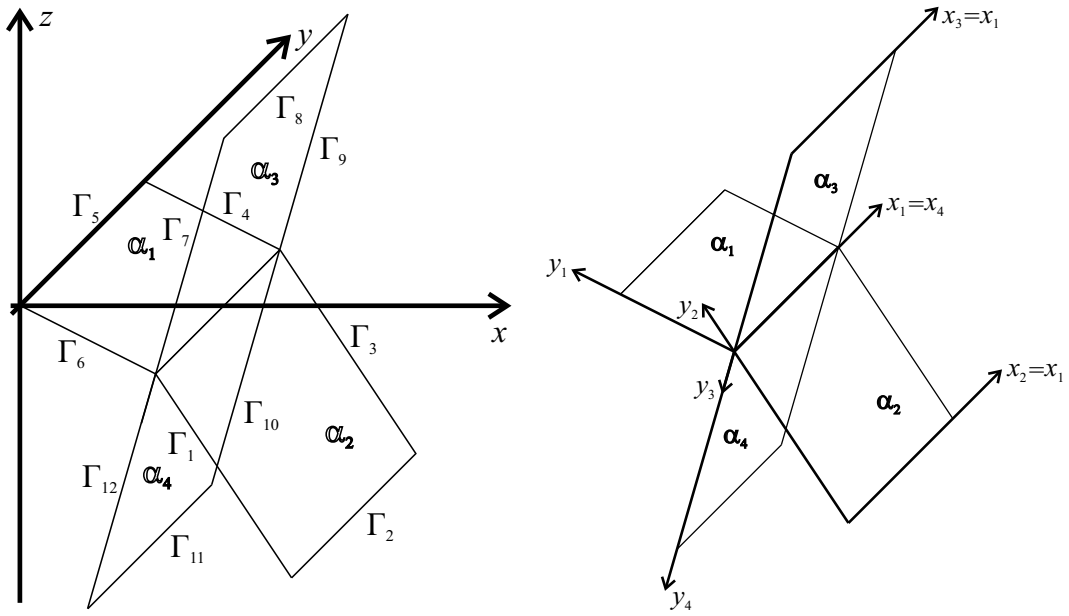

Fig. 3. System $\mathcal{S}$ for the model problems and coordinate systems in each polygon

7.1 Model problem with a known analytical solution

We consider two simple model problems in this section. The first model problem corresponds to the system $\mathcal{S}$ created by four rectangles as viewed in Figure 3. We verify on this problem the theoretical error estimates for the situation where the central edge is shared by four polygons. The second model problem is a simplification of the previous one, with just the rectangles α_1 and α_2 creating the system; there is no multiply shared edge in this case. Both model problems have the same known analytical solution in α_1 and α_2. We consider the second model problem in order to investigate the changes of the approximation error implied by the presence of a multiply shared edge. All the computations presented in this section were done in double precision on a personal computer with machine precision being in power of 10^{-16}. The resulting systems of linear equations were solved by the preconditioned conjugate gradients method.

The first model problem is given by:

$$\mathcal{S} = \overline{\alpha_1} \cup \overline{\alpha_2} \cup \overline{\alpha_3} \cup \overline{\alpha_4} \setminus \partial\mathcal{S}\,,$$

$$\begin{aligned} \mathbf{u} &= -(\nabla p + \nabla z) \quad \text{in } \alpha_i\,, i = 1,2,3,4\,, \\ \nabla \cdot \mathbf{u} &= 0 \quad \text{in } \alpha_i\,, i = 1,2,3,4\,, \end{aligned}$$

$$
\begin{gathered}
p = 0 \quad \text{on } \Gamma_1\,, \quad p = 0 \quad \text{on } \Gamma_2\,, \\
\mathbf{u}\cdot\mathbf{n} = 0 \quad \text{on } \Gamma_3\,, \quad \mathbf{u}\cdot\mathbf{n} = 0 \quad \text{on } \Gamma_4\,, \\
p = \sin\Big(\frac{\pi x_1}{2X}\Big)\sinh\Big(\frac{\pi(A+B)}{2X}\Big) + S\,A \quad \text{on } \Gamma_5\,, \quad p = S\,y_1 \quad \text{on } \Gamma_6\,, \\
p = 0 \quad \text{on } \Gamma_7\,, \quad p = 0 \quad \text{on } \Gamma_8\,, \\
\mathbf{u}\cdot\mathbf{n} = 0 \quad \text{on } \Gamma_9\,, \quad \mathbf{u}\cdot\mathbf{n} = 0 \quad \text{on } \Gamma_{10}\,, \\
p = \sin\Big(\frac{\pi x_4}{2X}\Big)\sinh\Big(\frac{\pi(B+B)}{2X}\Big) \quad \text{on } \Gamma_{11}\,, \quad p = 0 \quad \text{on } \Gamma_{12}\,,
\end{gathered}
$$

where $A = |\Gamma_4| = \sqrt{5}/4$, $X = |\Gamma_2| = 1$, $B = |\Gamma_3| = |\Gamma_9| = |\Gamma_{10}| = \sqrt{13}/4$, and $S = \partial z/\partial y_2 - \partial z/\partial y_1$. The geometry of this model problem is viewed in Figure 3. The exact solution can be found as

$$
\begin{aligned}
p|_{\alpha_1} &= \sin\Big(\frac{\pi x_1}{2X}\Big)\sinh\Big(\frac{\pi(y_1+B)}{2X}\Big) + S\,y_1\,, \\
\mathbf{u}|_{\alpha_1} &= \Big(-\frac{\pi}{2X}\cos\Big(\frac{\pi x_1}{2X}\Big)\sinh\Big(\frac{\pi(y_1+B)}{2X}\Big), \\
&\qquad -\frac{\pi}{2X}\sin\Big(\frac{\pi x_1}{2X}\Big)\cosh\Big(\frac{\pi(y_1+B)}{2X}\Big) - S - \frac{\partial z}{\partial y_1}\Big)\,, \\
p|_{\alpha_2} &= \sin\Big(\frac{\pi x_2}{2X}\Big)\sinh\Big(\frac{\pi y_2}{2X}\Big)\,, \\
\mathbf{u}|_{\alpha_2} &= \Big(-\frac{\pi}{2X}\cos\Big(\frac{\pi x_2}{2X}\Big)\sinh\Big(\frac{\pi y_2}{2X}\Big), -\frac{\pi}{2X}\sin\Big(\frac{\pi x_2}{2X}\Big)\cosh\Big(\frac{\pi y_2}{2X}\Big) - \frac{\partial z}{\partial y_2}\Big)\,, \\
p|_{\alpha_3} &= \sin\Big(\frac{\pi x_3}{2X}\Big)\sinh\Big(\frac{\pi y_3}{2X}\Big)\,, \\
\mathbf{u}|_{\alpha_3} &= \Big(-\frac{\pi}{2X}\cos\Big(\frac{\pi x_3}{2X}\Big)\sinh\Big(\frac{\pi y_3}{2X}\Big), -\frac{\pi}{2X}\sin\Big(\frac{\pi x_3}{2X}\Big)\cosh\Big(\frac{\pi y_3}{2X}\Big) - \frac{\partial z}{\partial y_3}\Big)\,, \\
p|_{\alpha_4} &= \sin\Big(\frac{\pi x_4}{2X}\Big)\sinh\Big(\frac{\pi(y_4+B)}{2X}\Big)\,, \\
\mathbf{u}|_{\alpha_4} &= \Big(-\frac{\pi}{2X}\cos\Big(\frac{\pi x_4}{2X}\Big)\sinh\Big(\frac{\pi(y_4+B)}{2X}\Big), \\
&\qquad -\frac{\pi}{2X}\sin\Big(\frac{\pi x_4}{2X}\Big)\cosh\Big(\frac{\pi(y_4+B)}{2X}\Big) - \frac{\partial z}{\partial y_4}\Big)\,.
\end{aligned}
$$

Note that the gradients of z in α_1 and α_2 are different. Hence the occurrence of the term S, which ensures the continuity of the normal trace of the velocity field. Table 1 gives the approximation errors in the first rectangle α_1. The system $\mathcal{S}$ is discretized into $4\times 2N^2$ regular triangular elements, $h \approx 1/N$. There is the expected $O(h)$ convergence of $\mathbf{u}_h$, $O(h)$ convergence of the elementwise constant p_h, and $O(h^2)$ convergence of the piecewise linear but discontinuous $\tilde{\lambda}_h$.

N	Triangles	$\|p - p_h\|_{0,\mathcal{S}}$	$\|p - \tilde{\lambda}_h\|_{0,\mathcal{S}}$	$\|\mathbf{u} - \mathbf{u}_h\|_{\mathbf{H}(\mathrm{div},\mathcal{S})}$
2	8×4	0.4445	0.1481	1.2247
4	32×4	0.2212	0.0389	0.6263
8	128×4	0.1102	0.0098	0.3150
16	512×4	0.0550	0.0025	0.1577
32	2048×4	0.0275	$6.18{\cdot}10^{-4}$	0.0789
64	8192×4	0.0138	$1.54{\cdot}10^{-4}$	0.0394
128	32768×4	0.0069	$3.87{\cdot}10^{-5}$	0.0197
256	131072×4	0.0034	$9.73{\cdot}10^{-6}$	0.0099

Table 1
Approximation errors in α_1, the first model problem

The second model problem is given by

$$\mathcal{S} = \overline{\alpha_1} \cup \overline{\alpha_2} \setminus \partial\mathcal{S}\,,$$

$$\begin{aligned} \mathbf{u} &= -(\nabla p + \nabla z) \quad \text{in } \alpha_i\,, i = 1,2\,, \\ \nabla \cdot \mathbf{u} &= 0 \quad \text{in } \alpha_i\,, i = 1,2\,. \end{aligned}$$

The boundary conditions on Γ_1–Γ_6 are given as in the previous case. Also the exact solution in α_1 and α_2 stays unchanged. Table 2 gives the approximation errors in the first rectangle α_1 for this model problem. As the exact solution in α_1 coincides with that of the first model problem, we can compare these results with that of Table 1. The difference in approximation error is very small even for rough triangulations and disappears for increasing N. Hence a confirmation of the conclusions outlined by the theory: the presence of multiply shared interpolygon boundaries does not influence the approximation properties of the lowest-order Raviart–Thomas mixed finite element method.

7.2 Real problem

We present the simulation of fracture flow around the explorational drill hole Ptp-3 in the granitoid massif of Potůčky, Western Bohemia, in this section and compare our method with other approaches.

There exists a large variety of approaches to modeling the flow through a network of polygonal disks representing the rock fractures. In [8,10,14] the networks of polygonal disks are replaced by networks of one-dimensional pipes. This allows for fast

N	Triangles	$\|p-p_h\|_{0,\mathcal{S}}$	$\|p-\tilde{\lambda}_h\|_{0,\mathcal{S}}$	$\|\mathbf{u}-\mathbf{u}_h\|_{\mathbf{H}(\mathrm{div},\mathcal{S})}$
2	8×2	0.4481	0.1496	1.2236
4	32×2	0.2212	0.0393	0.6262
8	128×2	0.1102	0.0099	0.3150
16	512×2	0.0550	0.0025	0.1577
32	2048×2	0.0275	$6.24{\cdot}10^{-4}$	0.0789
64	8192×2	0.0138	$1.56{\cdot}10^{-4}$	0.0394
128	32768×2	0.0069	$3.90{\cdot}10^{-5}$	0.0197
256	131072×2	0.0034	$9.76{\cdot}10^{-6}$	0.0099

Table 2
Approximation errors in α_1, the second model problem

calculations with large networks, but the precision is compromised. The models proposed in [2,4,11,13,21] discretize the polygonal networks into triangular or quadrilateral meshes. Because of a very complex geometry, the number of mesh elements is often sizably increased. Finite difference, finite volume, finite element, or boundary element methods are used for the discretization. We refer e.g. to [6] for a more detailed survey.

Our intention in the simulation of a real problem was twofold. First, we have constructed a very accurate mesh of the fracture network, which had at the same time as few elements as possible. Second, we have used the mixed finite element method studied in this paper for the discretization of the fracture flow problem. We have first approximated the real fractures by a system of polygons generated on the basis of the results of field measurements from [15]. We have next computed the intersections of the polygons. In order to simplify the system of intersections in each polygon, these were slightly moved and stretched in the polygon planes. This allowed for a significant decrease of the number of triangular elements necessary to discretize each polygon and for an improvement of their shapes. The triangular mesh had to respect the system of intersections in each polygon, but as a consequence of the simplifications made, the interpolygon geometrical correspondence vanished. This was replaced with an element edges correspondence: the corresponding edges in different polygons did not necessarily have to match geometrically—only what was the outflow from one triangular element through a given edge had to be the inflow into the neighboring ones through the edges that were associated with the given one. Such "mass balance" correspondence is completely sufficient to implement the mixed finite element method. Finally, based on the assigned aperture, fracture wall roughness, and filling, the hydraulic permeability of each triangular element was set. We have thus avoided the classical parallel plate model.

The optimized triangulation of the fracture network and the model allowing for variable permeability inside the fractures together with the mixed finite element method

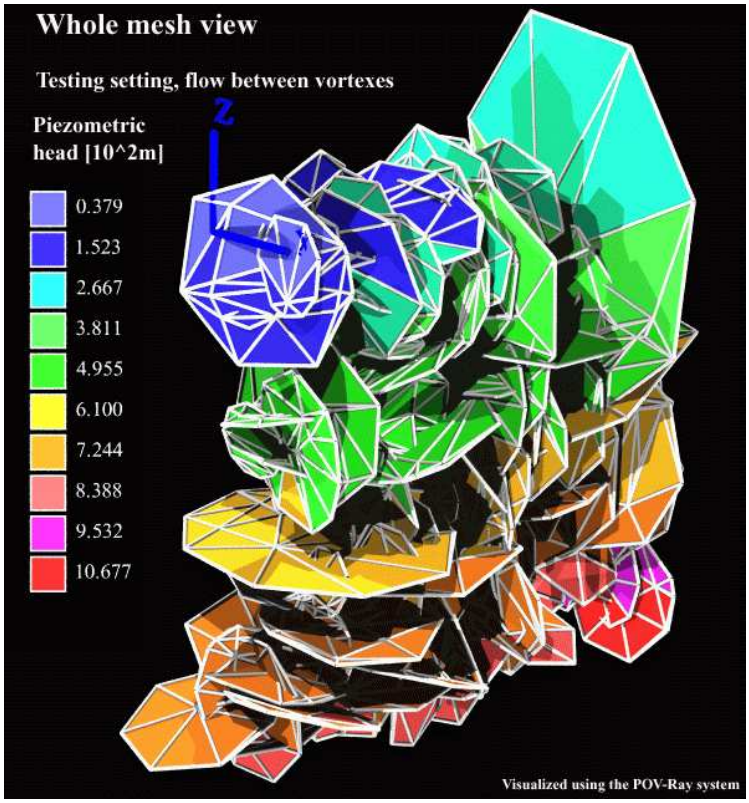

Fig. 4. Distribution of the piezometric head in a fracture network

ensuring the mass balance in each element even for meshes with no real geometrical correspondence have proved a good agreement between observed phenomena and the numerical approximation. The model gave an accurate velocity field within fracture planes and thus in the whole simulated network. Namely, the channeling effect was successfully simulated both in fracture planes and in the entire network. This effect is given by the fact that the natural three-dimensional fractures have varying apertures and consequently the flow is not evenly distributed within the fracture planes. All these results are described in detail in [17]. We only give here in Figure 4 an example of the distribution of the piezometric head in the simulated fracture network.

Acknowledgements

The first author wants to thank Professor Christian Grossmann from the Dresden University of Technology for his useful advice and hints.

References

[1] Adler P.M., Thovert J.-F., *Fractures and Fracture Networks*, Kluwer, Dordrecht, 1999.

[2] Andersson J., Dverstorp B., Conditional simulations of fluid flow in three-dimensional networks of discrete fractures, *Water Resour. Res.* **23** (1987), 1876–1886.

[3] Arnold D.N., Brezzi F., Mixed and nonconforming finite element methods: Implementation, postprocessing and error estimates, *RAIRO Modél. Math. Anal. Numér.* **19** (1985), 7–32.

[4] Bastian P., Chen Z., Ewing R.E., Helmig R., Jakobs H., Reichenberger V., Numerical simulation of multiphase flow in fractured porous media, in Chen Z., Ewing R.E., Shi Z.C. eds., *Numerical Treatmenet of Multiphase Flows in Porous Media*, pp. 50–68, Springer-Verlag, Berlin, 2000.

[5] Bear J., Modeling flow and contaminant transport in fractured rocks, in Bear J., Tsang C.F., de Marsily G. eds., *Flow and Contaminant Transport in Fractured Rock*, pp. 1–38, USA: Academic Press, 1993.

[6] Bogdanov I.I., Mourzenko V.V., Thovert J.-F., Adler P.M., Effective permeability of fractured porous media in insteady state flow, *Water Resour. Res.* **39** (2003), 1023, doi:10.1029/2001WR000756.

[7] Brezzi F., Fortin M., *Mixed and Hybrid Finite Element Methods*, Springer-Verlag, New York, 1991.

[8] Cacas M.C., Ledoux E., de Marsily G., Tillie B., Barbreau A., Durand E., Feuga B., Peaudecerf P., Modeling fracture flow with a stochastic discrete fracture network: Calibration and validation 1. The flow model, *Water Resour. Res.* **26** (1990), 479–489.

[9] Chen Z., Equivalence between and multigrid algorithms for nonconforming and mixed methods for second-order elliptic problems, *East-West J. Numer. Math.* **4** (1996), 1–33.

[10] Dershowitz W.S., Fidelibus C., Derivation of equivalent pipe network analogues for three-dimensional discrete fracture networks by the boundary element method, *Water Resour. Res.* **35** (1999), 2685–2691.

[11] Elsworth D., A hybrid boundary element-finite element analysis procedure for fluid flow simulation in fractured rock masses, *Int. J. Numer. Anal. Methods Geomech.* **10** (1986), 569–584.

[12] Hoteit H., Erhel J., Mosé R., Philippe B., Ackerer Ph., Numerical reliability for mixed methods applied to flow problems in porous media, *Comput. Geosci.* **6** (2002), 161–194.

[13] Koudina N., Gonzalez Garcia R., Thovert J.-F., Adler P.M., Permeability of three-dimensional fracture networks, *Phys. Rev. E* **57** (1998), 4466–4479.

[14] Long J.C.S., Gilmour P., Witherspoon P.A., A model for steady state flow in random three dimensional networks of disc-shaped fractures, *Water Resour. Res.* **21** (1985), 1105–1115.

[15] Maros G., Palotás K., Koroknai B., Sallay E., Szongoth G., Kasza Z., Zilahi-Sebess L., Core log evaluation of borehole Ptp-3 in the Krušné hory mts, MS Geological Institute of Hungary, Budapest, 2001.

[16] Maryška J., Severýn O., Vohralík M., Mixed-hybrid FEM discrete fracture network model of the fracture flow, in Sloot P. M. A. et al. eds., *Proceedings of Computational Science - ICCS 2002*, pp. 794–803, Springer, Amsterdam, 2002.

[17] Maryška J., Severýn O., Vohralík M., Numerical simulation of fracture flow with a mixed-hybrid FEM stochastic discrete fracture network model, *Comput. Geosci.* **8** (2004), 217–234.

[18] Quarteroni A., Valli A., *Numerical Approximation of Partial Differential Equations*, Springer-Verlag, Berlin, 1994.

[19] Raviart P.-A., Thomas J.-M., A mixed finite element method for 2-nd order elliptic problems, in Galligani I., Magenes E. eds., *Mathematical Aspects of Finite Element Methods*, Lecture Notes in Math. 606, pp. 292–315, Springer, Berlin, 1977.

[20] Roberts J.E., Thomas J.-M., Mixed and hybrid methods, in Ciarlet P.G., Lions J.L. eds., *Handbook of Numerical Analysis*, vol. 2, pp. 523–639, Elsevier Science B.V., Amsterdam, 1991.

[21] Slough K.J., Sudicky E.A., Forsyth P.A., Numerical simulations of multiphase flow and phase partitioning in discretely fractured geological media, *J. Contam. Hydrol.* **40** (1999), 107–136.

[22] Thomas J.-M., Sur l'analyse numérique des méthodes d'éléments finis hybrides et mixtes, Ph.D. Dissertation, Université Pierre et Marie Curie (Paris 6), 1977.

[23] Vohralík M., Maryška J., Severýn O., Mixed-hybrid discrete fracture network model, in Chen Z., Glowinski R., Li K. eds., *Current Trends in Scientific Computing*, Contemporary Mathematics, Volume **329**, pp. 325–332, American Mathematical Society, 2003.

[24] Wanfang Z., Wheater H.S., Johnston P.M., State of the art of modelling two-phase flow in fractured rock, *Envir. Geol.* **31** (1997), 157–166.